15TH IEA HEAT PUMP CONFERENCE
MAY 26–29, 2026 | HOFBURG
VIENNA 2026
DECARBONISATION THROUGH INNOVATION

A High-Temperature Tri-Phase Thermochemical Heat Pump for Industrial Process Heating

Rundong Chen [a, b], Ding Lu [a, b, c, **], Tao Shen [a, b], Maoqiong Gong [a, b, *]

[a] *State Key Laboratory of Cryogenic Science and Technology, Technical Institute of Physics and Chemistry, Chinese Academy of Sciences, Beijing 100190, China*
[b] *University of Chinese Academy of Sciences, Beijing 100049, China*
[c] *Institute of Optical Physics and Engineering Technology, Qilu Zhongke, Jinan 251000, China*
[*] *Corresponding author. State Key Laboratory of Cryogenic Science and Technology, Technical Institute of Physics and Chemistry, Chinese Academy of Sciences, Beijing, 100190, China.*
[**] *Corresponding author. State Key Laboratory of Cryogenic Science and Technology, Technical Institute of Physics and Chemistry, Chinese Academy of Sciences, Beijing, 100190, China.*

Abstract

Thermochemical heat pumps have attracted widespread attention due to their capability to provide flexible energy conversion and regulation in intelligent energy networks. However, conventional two-phase absorption systems, such as LiBr-H_2O, are intrinsically constrained by crystallization, which fundamentally limits their achievable temperature lift and operational flexibility. To overcome these limitations, this work proposes a new tri-phase thermochemical heat pump system in which solid phase participation extends the thermochemical conversion pathway beyond conventional two-phase cycles. By integrating sensible heat, latent heat, and thermochemical energy, the system enables high density energy conversion and a large temperature lift. A thermodynamic model is developed to describe the interaction principles among the three phases. A comprehensive evaluation methodology is established to analyze the effects of key parameters. Results show that the introduction of the solid phase leads to a significant improvement in system performance, with discharge temperatures exceeding 140 °C. Specifically, the energy efficiency is enhanced by up to 19.5%, and the exergy efficiency is increased by up to 34.2%. The system achieves a maximum temperature lift of 60 °C. Additionally, the heat release per unit mass of the salt has increased by 2.6 times, indicating the system capacity of large-scale thermal energy regulation and conversion. Furthermore, an innovative microencapsulation design is proposed to eliminate the risks of blockage and corrosion, consequently ensuring stable tri-phase operation. Overall, the proposed system provides a significant performance breakthrough over conventional cycles, thereby supporting the transition toward industrial decarbonization.

Keywords: thermochemical heat pump, tri-phase, temperature lift, exergy efficiency, microencapsulation ;

1. Introduction

Industrial heat demand constitutes a major share of heat consumption globally, predominantly supplied by fossil fuels,chiefly coal and natural gas,resulting in high carbon emissions, inadequate utilization, and suboptimal efficiency[1]. According to the *Net Zero by 2050: A Roadmap for the Global Energy Sector* published by the IEA, the Net Zero Scenario projects that heat pumps provide about 30% of total heat demand in light industries by 2050. This highlights the imperative to develop high-temperature, high-efficiency, and flexible advanced heat pump technologies to support industrial decarbonization.

Absorption heat pumps, including absorption heat transformers, are thermally driven by low-grade heat such as industrial waste heat and renewable heat sources[2-4]. They are therefore widely regarded as one of the key pathways for decarbonising industrial process heat. Most research worldwide has primarily focused on cycle modifications, including dual-/multistage configurations and hybrid absorption – compression schemes, to expand the attainable lift and attain high temperature output[5]. Ma et al.[6] compared alternative cycle configurations and noted that, although two-stage systems can deliver a temperature lift (Δ T) of 31.8-68.6 ℃, this is often achieved at the expense of the coefficient of performance. Ji et al. [7] further

[*] Corresponding author. Tel.: 010-82543728
E-mail address: E-mail addresses: luding@mail.ipc.ac.cn (D. Lu), gongmq@mail.ipc.ac.cn (M. Gong).

15th IEA Heat Pump Conference 2026 - HTH5.2 - https://doi.org/10.23697/vn9y-3g22

showed that two-stage cycles, while raising the outlet temperature, are highly sensitive to interstage heat exchange and solution splitting. As the number of stages increases, multistage systems can further extend the temperature lift; however, the added cycle loops and heat exchange units increase structural complexity and costs, while reducing reliability and operability [8]. Beyond staged cycles, absorption-compression hybrid configurations have been proposed to achieve higher outlet temperatures [9]. Feng et al. [10] achieved a 50 ℃ temperature lift by using a mass coupling strategy, whereas Gao et al. [11] realized a maximum 54 ℃ lift via thermal coupling while maintaining a COP of 1.8. Compared with two-/multistage absorption systems, such hybrids can improve COP, yet they depend on high quality electricity, introduce additional components, and control complexity[12], which constrains their engineering deployment. However, conventional two-phase (gas-liquid) absorption heat pumps face inherent bottlenecks under high-temperature, large-lift operation [13, 14]. Achieving large temperature lift hinges on the solution concentration glide, but excessive concentrations trigger on working fluid crystallization and channel plugging. In addition, high temperature and high-concentrated solutions significantly accelerate materials degradation and corrosion. These results motivate the pursuit of multiphase mechanisms, a transition from two to three phases, whereby introducing a crystalline solid phase affords high-grade heat release and enhanced controllability.

Current research on gas-liquid-solid three-phase systems has been concentrated predominantly in thermochemical energy storage (TCES), whereas exploration within the heat pump domain remains comparatively limited. Compared with sensible and latent energy storage, TCES relies on differences in chemical potential to mediate charging and discharging, offers superior storage density, minimal heat loss, and controllable heat quality, and has therefore attracted broad attention [15]. Three-phase thermochemical energy storage has evolved as an extension of conventional gas-liquid absorption energy storage, typically employing strong hygroscopic salts and water as working pairs such as H_2O-LiBr/LiCl/$CaCl_2$ [16]. The core principle is to introduce a crystalline solid phase, so that it exploits deliquescence and dehydration heats in addition to absorption, which markedly extend the concentration glide and deliver higher energy storage density. The simulation studies converge on the high energy storage density (ESD) advantage of three phase TCES system. Using the LiCl-H_2O working pair, Yu et al. [17] reported that introducing crystallization can increase storage density by 260%,with subsequent dehydration providing a further 46% improvement. For a long-duration LiCl-H_2O thermochemical storage system, N’ T soukpoe et al. [18] demonstrated that increasing the crystallization fraction can deliver more than a threefold improvement in storage density compared with conventional systems, with a storage efficiency up to 0.9. In an open three-phase configuration using LiCl crystalline hydrates, Wang et al. [19] achieved high concentration operation with cooling-induced crystallization during charging, and released energy through crystal dissolution during discharging, yielding a volumetric storage density of 300 kWh/m^3. Furthermore, You et al. [20]incorporated an electric-rod melting unit together with a water-flushing module; at a crystallization fraction of 0.4144, the system attained 220 kWh/m^3. Despite these advances, most studies remain restricted to charging at 60-100 ℃ and discharging at 30-50 ℃ [21, 22], primarily emphasizing storage density and efficiency. In contrast, the high-temperature regime and the potential for actively controllable heat release have received comparatively limited attention.

Based on the aforementioned challenges, this study proposes a high-temperature tri-phase thermochemical heat pump (TCTP). The novelty is to introduce a solid crystalline phase into the conventional gas-liquid cycle, expanding the concentration glide through crystallization-redissolution and hydration-dehydration reactions, and eventually realize large temperature lift and high temperature output. A thermodynamic model is established by coupling Aspen Plus and MATLAB. Furthermore, the evaluation indicators are refined by explicitly incorporating heat grade, enabling a more comprehensive assessment of the system characteristics. By analyzing the influence of key operating parameters, a theoretical foundation is established for the optimization of tri-phase thermochemical heat pumps, with the aim of realizing a high efficiency heat pump system for industrial process heating.

2. Methodology

In this section, a theoretical analysis of tri-phase thermochemical heat pumps is illustrated. On this basis,a thermodynamic cycle model is formulated to characterize the coupled phase-change and reaction processes throughout the cycle. To enable a comprehensive evaluation of system performance, an indicator reflecting heat grade is introduced to quantify energy quality. This framework serves as the foundation for the subsequent parametric analysis.

2.1. Thermodynamic analysis

As illustrated in Fig. 1, the thermodynamic cycle of the tri-phase thermochemical heat pump can be interpreted on a *p-T-x* diagram. As described in Eq.(1), the sorbent and sorbate are separated in point A driven by an external heat source. And the sorbate is condensed into liquid water in point E. With the increase of heat grade, the separation is further extended, the sorbent sequentially evolves from a weak solution to a concentrated and saturated solution, and eventually forms a crystalline solid salt, corresponding to the transition from point A to point D. The charging temperature is therefore determined by the condensation pressure, which is a function of the condensation temperature. As described in Eq.(2), during the discharging stage, liquid water evaporates into vapor and is subsequently taken up by the sorbent, releasing heat. The discharging temperature is governed by the evaporation pressure, which in turn depends on the evaporation temperature. As the process continues, the sorbent reverses through the crystalline solid, saturated solution, and concentrated solution states, and finally returns to the weak solution condition.

$$AB + \Delta H \rightarrow A + B \tag{1}$$

$$A + B \rightarrow AB + \Delta H \tag{2}$$

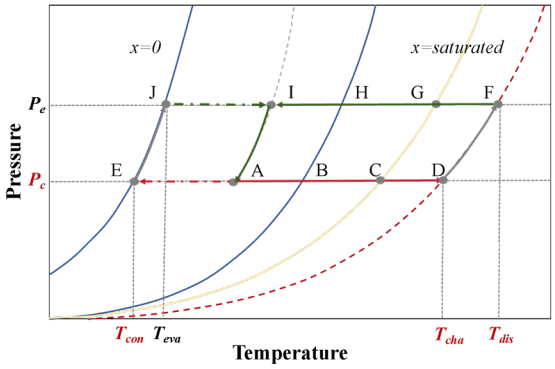

Fig. 1 Thermodynamic cycle of tri-phase thermochemical heat pump.

To realize the foregoing thermodynamic cycle, a tri-phase continuous thermochemical heat pump is developed， in which two reactor beds are operated in coordinated, alternating modes by valve switching. When Reactor A serves as the generator, Valves 1 and 4 are opened and Valves 2 and 3 are closed. Concurrently, Reactor B is performing as vapor uptake and heat release. Upon switching, Reactor B becomes the generator, with Valves 2 and 3 opened and Valves 1 and 4 closed, when the sorbent takes up vapor from the sorbate to supply high-grade heat in Reactor A. By alternating the roles of the two beds with the prescribed valve sequence, the system achieves seamless relay operation and a stable, continuous high-temperature output.

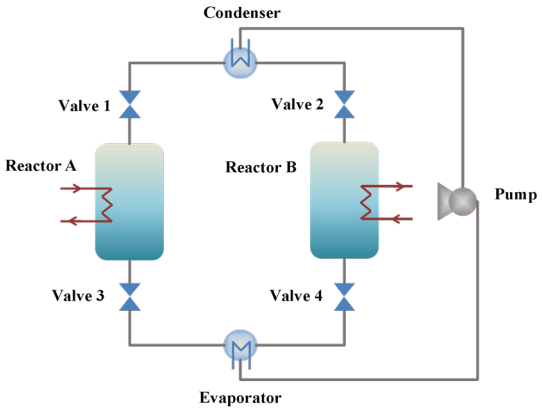

Fig. 2 Schematic of a high-temperature continuous TCTP.

Because distinct characteristics are imparted by different working pairs, variations in system performance and operational behavior are observed under identical conditions. Nevertheless, these systems are governed by common underlying principles, so insights obtained from a single working pair are broadly generalizable to others. In this study, $CaCl_2$-H_2O is chosen as the representative pair owing to its low cost, well-characterized thermodynamic properties, and favorable cycling stability.

In Fig. 1, both the A-C and G-I segments lie in the vapor-liquid two-phase region, where the working pair is $CaCl_2$ solution and water, as seen in Eq.(4). The temperature-pressure-concentration (*T*-*p*-*x*) relationship is described using the Pitzer theory. The solution water activity is evaluated and the equilibrium is expressed as Eq. (3).

$$p = a_w(x,T)\,p_{sat}(T) \tag{3}$$

Where $p_{sat}(T)$ denotes the saturation vapor pressure of pure water. Accordingly, for a specified solution concentration, the operating temperature can be determined by inverting the above relation. This provides a unified thermodynamic method for quantitative state identification and path calculation within the two-phase region. Points C and G are identified as three-phase equilibrium points, corresponding to crystallization and deliquescence, respectively, as depicted in Eq.(5). Furthermore, the C-D and F-E segments are governed by hydration and dehydration of the crystalline salt. These reactions proceed through several discrete hydration levels, which are summarized in Eqs. (6)~(8). Under high-temperature operating conditions, a temperature-correction term is introduced to improve the accuracy of the pressure-temperature correlation, as presented in Eq. (9).

$$\mathrm{CaCl_2\ strong\ solution(aq)} + \mathrm{H_2O(g)} \leftrightarrow \mathrm{CaCl_2\ weak\ solution\ (aq} \tag{4}$$

$$\mathrm{CaCl_2 \cdot 2H_2O(s) + H_2O(g) \leftrightarrow CaCl_2\ saturated\ solution\ (aq} \tag{5}$$

$$\mathrm{CaCl_2 \cdot 2H_2O(s) \leftrightarrow CaCl_2 \cdot H_2O(s) + H_2O(g)} \tag{6}$$

$$\mathrm{CaCl_2 \cdot H_2O(s) \leftrightarrow CaCl_2 \cdot \frac{1}{3}H_2O(s) + \frac{2}{3}H_2O(g)} \tag{7}$$

$$\mathrm{CaCl_2 \cdot \frac{1}{3}H_2O(s) \leftrightarrow CaCl_2(s) + \frac{1}{3}H_2O(g)} \tag{8}$$

$$\begin{aligned} \ln(P/P^0) &= \frac{\Delta S^0}{R} - \frac{\Delta H^0}{RT} \\ &= -\frac{\Delta H^0_{298.15}}{RT} - \frac{\int_{298.15}^{T} \Delta C_p^0 dT}{RT} + \frac{\Delta S^0_{298.15}}{R} + \frac{1}{R}\int_{298.15}^{T} \frac{\Delta C_p^0}{T} dT \\ &= \frac{\Delta S^0_{298.15}}{R} - \frac{\Delta H^0_{298.15}}{RT} - \ln\left(\frac{T}{298.15}\right) + 1 - \frac{298.15}{T} \\ &= \frac{A}{RT} + B - \ln\left(\frac{T}{298.15}\right) + 1 - \frac{298.15}{T} \end{aligned} \tag{9}$$

In this section, a systematic thermodynamic description of the TCTP system has been established, and a quantitative characterization has been performed on the basis of the intrinsic properties of the working pair, complemented by multiple thermodynamic analysis methods. The analysis provides a complete theoretical basis for the subsequent model development.

2.2. Simulation method

An integrated thermodynamic model is developed to uniformly describe the gas-liquid absorption/desorption, gas-liquid-solid crystallization/redissolution, and gas-solid hydration/dehydration processes within the cycle. MATLAB and Aspen are computationally coupled through the COM interface, through which parameter adjustment and performance evaluation under various operating conditions are achieved. With this model and the proposed evaluation indicators, the effects of key operating parameters on the TCHP system are elucidated, thereby providing theoretical support for system design and operational optimization.

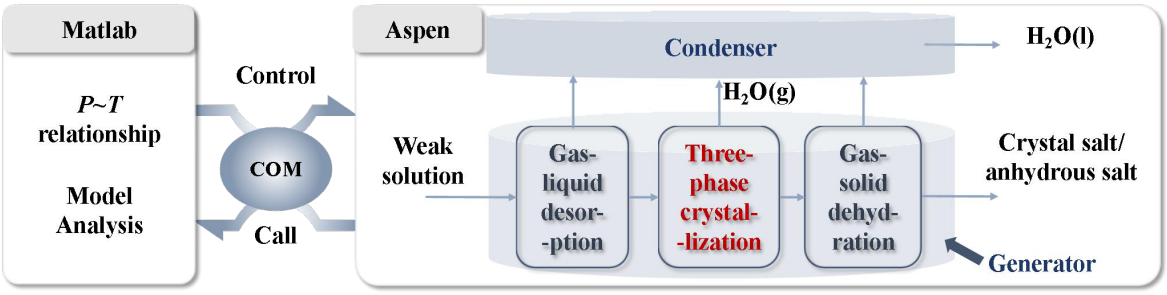

Fig. 3 Schematic diagram of MATLAB-Aspen coupled computation.

2.2.1. *Thermodynamic models*

Considering the distinct reaction characteristics in different regions of the system, appropriate thermodynamic models were selected to describe the corresponding behaviors. All models were developed in accordance with the principles of mass, species, and energy conservation [23] , as seen in Eqs.(10)~(12).

$$\sum m_{in} - \sum m_{out} = 0 \tag{10}$$

$$\sum (mx)_{in} - \sum (mx)_{out} = 0 \tag{11}$$

$$\sum (mh)_{in} - \sum (mh)_{out} + Q + W = 0 \tag{12}$$

For the distinct processes occurring inside the reactor, appropriate Aspen unit models were employed to describe gas-liquid behavior, gas-liquid-solid equilibria, and gas-solid processes, thereby enabling an accurate representation of the reaction and phase-transition behavior.

Table 1. Thermodynamic modeling in Aspen.

Models			Modules
Charging	Condenser		HEATER
	Reactor	Gas-liquid desorption	FLASH
		Three-phase crystallization	FLASH
		Gas-solid desorption	RGIBBS
	Evaporator		HEATER
	Throttle valve		VALVE
Discharging	Reactor	Gas-liquid absorption	HEATER
		Three-phase deliquescence	HEATER
		Gas-solid adsorption	RGIBBS

2.2.2. *Model validation*

To validate the accuracy of the proposed model, experimental data on three-phase thermochemical energy storage reported by You et al. [20] are adopted. The crystallization performance of the system was characterized by the crystallization ratio (r), defined as the molar fraction of LiCl crystals in the total amount of sorbent material, as shown in Eq.(13).

In order to ensure that the model is validated under realistic conditions, the operating parameters and boundary conditions were carefully selected to match those used in the experiments. These parameters, as shown in Table 2. It is important to note that the boundary conditions and system design used in the model were explicitly aligned with the experiment to ensure consistency and reproducibility. This alignment is critical for accurately comparing the results from the model with the experimental data. The model produced results with a maximum deviation of 9.58%, as shown in Table 3. It is essential to recognize that slight discrepancies between the model and experimental results are often expected due to idealization and simplifications in the modeling process.The relatively small deviation further supports the reliability of the

model and confirms its ability to accurately simulate the energy conversion under the specified conditions.These results demonstrate the validity and accuracy of the developed model.

$$r = \frac{n_{\mathrm{LiBr\cdot H_2O}}}{n_{\mathrm{LiBr}}} \tag{13}$$

Table 2. Operating parameters of the experiment.

Output temperature (℃)	Heat source temperature (℃)	Ambient temperature during charging (℃)	Ambient temperature during discharging (℃)
45	90	15	15

Table 3.Model validation.

Parameter		Result (simulation)	Result (reference)	Deviation
Charging	Q_{in}	132.9 kWh	124.5 kWh	6.74%
	r (after crystallization stage)	0.4101	0.4144	1.05%
Discharging	Q_{out}	110.6 kWh	100.9 kWh	9.58%
	r (before discharging process)	0.4690	0.4322	8.51%
Cycle	Energy efficiency	0.832	0.81	2.71%

2.2.3. Evaluation indicators

To enable a comprehensive quantitative assessment of the proposed TCHP, the coefficient of performance (COP) and the exergy efficiency (η_{EX}) are employed, so that the control of heat quantity and heat quality can be evaluated separately, as seen in Eqs.(14) and(15). For high-temperature heat pumps targeting industrial process heat, the heat output temperature is a key indicator of the system supply capability. Accordingly, it is introduced explicitly through an exergy formulation, as seen in Eq. (16), rather than being assessed solely under the first law of thermodynamics. This evaluation scheme is intended to provide a solid foundation for performance investigation.

$$COP = \frac{Q_{output}}{Q_{input}} = \frac{Q_{dis}}{Q_{eva} + Q_{cha}} \tag{14}$$

$$\eta_{EX} = \frac{E_{x,output}}{E_{x,input}} = \frac{E_{Q,dis}}{E_{Q,eva} + E_{Q,cha}} \tag{15}$$

$$E_Q = Q(1 - T_0 / T) \tag{16}$$

3. System analysis

In this section, three key parameters are investigated to discuss their influence on the system performance. The selection of parameters is based on the aforementioned thermodynamic analysis and practical operation conditions. These characteristics would guide the optimization of the TCHP system.

3.1. Charging process

3.1.1. Charging temperature

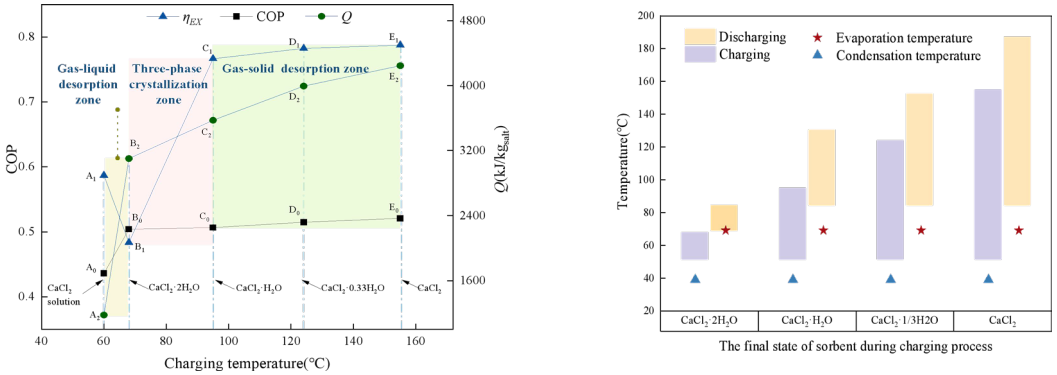

(a) Variation of COP , Q and η_{EX}.

(b) Distribution of operation temperature.

Fig. 4 Effects of charging temperature on system performance.

During the charging stage, the charging temperature is the primary governing parameter and directly determines the terminal state of the working pair in this phase. As shown in Fig. 4 (a), points A-E represent distinct charging states, and the subscripts 0-2 denote the COP, the exergy efficiency , and the heat released per unit mass of salt, respectively. Increases in charging temperature are found to induce successive changes in the sorbent state, which in turn exert a pronounced impact on system performance. When the charging temperature is raised from 60 ℃ to approximately 160 ℃, the COP is markedly increased; the most significant rise is observed at point B_0, which corresponds to the first appearance of a crystalline solid salt. Upon further dehydration, the sorbent is ultimately converted into the anhydrous salt at point E_0, where the COP reaches its maximum.

Compared with the conventional two-phase cycle, the incorporation of the solid phase results in substantial performance gains: the COP exhibits a 19.5% improvement, the heat released per unit mass of salt increases by a factor of 2.6, and the exergy efficiency increases by 34.2%. These results quantitatively demonstrate the superiority of the tri-phase thermochemical cycle in both heat quantity and heat quality enhancement.

Although the amount of thermal energy delivered by the TCHP increases monotonically, its quality does not follow the same trend. When the terminal state is $CaCl_2{\cdot}2H_2O$, a marked decrease in η_{EX} is observed. This is because $CaCl_2{\cdot}2H_2O$ is a crystallization product, so the subsequent discharging stage is initiated by deliquescence, which is constrained by ambient relative humidity and is passively triggered rather than actively regulated. Consequently, the heat-output temperature is lower, leading to a reduction in η_{EX}. This behavior is reflected in Fig. 4(b), where the temperature lift is the lowest among the terminal states. By contrast, when the terminal state is $CaCl_2{\cdot}2H_2O$, the overlap between the charging and discharging temperature ranges is minimized, and when the terminal state is anhydrous $CaCl_2$, the output temperature exceeds 180 ℃, which is higher than that for the other states.

For practical industrial heat supply applications, the $CaCl_2{\cdot}H_2O$ state offers the most appropriate balance between heat grade, controllability, and engineering feasibility. It provides a sufficiently high discharge temperature while avoiding the limitations of deliquescence and the operational challenges associated with achieving a fully anhydrous state.

3.1.2. Condensation temperature

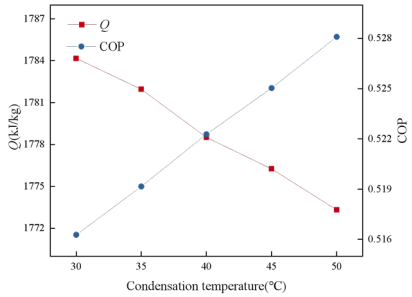

(a) Variation of COP and Q.

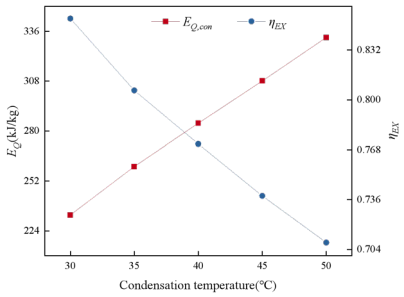

(b) Variation of E_Q and η_{EX}.

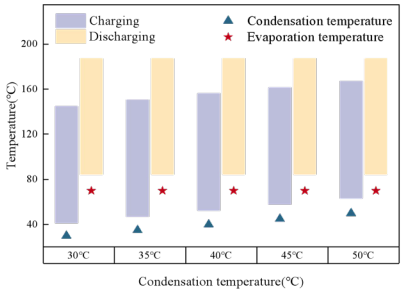

(c) Distribution of operating temperature.

Fig. 5 Effects of condensation temperature on system performance.

The condensation temperature is regarded as the parameter that determines the condensation pressure, which in turn defines the charging pressure, and thus directly influences the required heat grade for different terminal states during the charging process. As the condensation temperature increases, the heat quantity and heat quality required for charging exhibit different trends. For the TCHP cycle, the initial charging state is defined by the saturation temperature of the weak solution. A higher charging pressure implies a higher initial charging temperature; however, although the final charging temperature is also elevated, the amount of working pair that must be heated decreases progressively during charging. As a result, the total heating demand is reduced, and the COP is increased, as seen in Fig. 5(a).

On the other hand, because the heat grade is raised with increasing condensation temperature, the exergy of the supplied heat shows an increasing trend, which in turn leads to a reduction in η_{EX}, as depicted in Fig. 5(b). The influence of condensation temperature on the system COP is relatively limited, whereas its effect on the temperature lift is pronounced. When the condensation temperature is set to 30 ℃, the overlap between the charging and discharging temperature ranges is minimized, indicating a strong temperature-lift capability,as shown in Fig. 5(c). For example, when the evaporation temperature is fixed at 80 ℃, the achievable temperature lift exceeds 60 ℃.

3.2. Discharging process

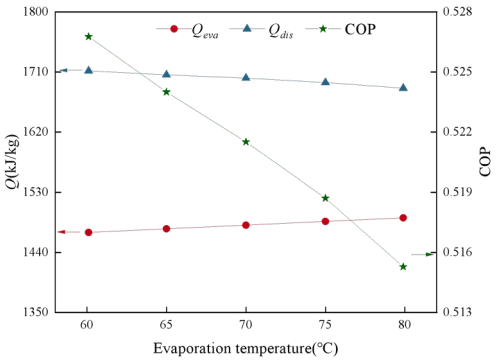

(a) Variation of COP and Q.

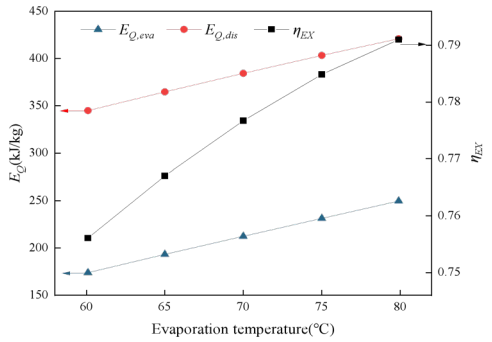

(b) Variation of E_Q and η_{EX}.

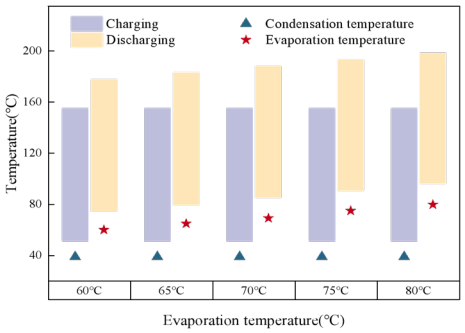

(c) Distribution of operating temperature.

Figure. 6 Effects of condensation temperature on system performance.

The discharging temperature is determined by the operating pressure, which is defined by the evaporation pressure and thus uniquely specified by the evaporation temperature. As shown in Fig. 6 (a) and Fig. 6 (b), the evaporation temperature directly affects both the total evaporation heat and its exergy. As the evaporation temperature increases, the discharging temperature exhibits an upward trend, whereas the total heat released by the system decreases, leading to a reduction in COP. This occurs because a portion of the hydration heat is consumed to raise the sensible temperature of the working pair, thereby reducing the net heat available for external supply.

From the perspective of the second law of thermodynamics, however, the exergy of heat release increases markedly as a consequence of the elevated heat grade during the discharging process. Although the exergy of evaporation also increases, its magnitude remains considerably lower than that of the released heat, resulting in a pronounced improvement in η_{EX}. Specifically, when the evaporation temperature increases from 60 ℃ to 80 ℃, the discharging temperature shows a clear upward trend, as shown in Fig. 6 (c), and the exergy of heat release improves by 22.0%, despite a modest 1.52% decrease in the total released heat. These results reveal a substantial enhancement in the heating quality of the TCHP system.

4. Application scheme

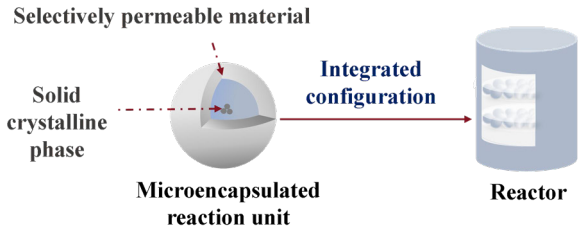

Figure. 7 Engineering design scheme for practical application of the TCHP system.

Although the theoretical analysis and model-based simulations have provided clear evidence that the TCHP system delivers a pronounced performance enhancement over conventional two-phase systems, the intrinsic complexity of the tri-phase behavior remains a major barrier to practical deployment. Previous studies have investigated several reactor configurations, which may generally be categorized into two types, by means of composite materials and forced separation, respectively. These configurations have enabled relatively stable operation of the tri-phase system. However, the risks of corrosion and blockage have not been fully eliminated.

To overcome these limitations, an innovative microcapsule scheme is proposed in this work. By coating the hygroscopic salt with a selectively permeable material, the formation and evolution of the crystalline solid phase can be effectively controlled. Water vapor is allowed to permeate freely through the coating, whereas the salt solution is confined within the microcapsule. As a result, the crystalline phase is generated internally, thereby effectively avoiding blockage and corrosion. As illustrated in Fig. 7, these microcapsules, regarded as the fundamental reaction units, are integrated and uniformly arranged within the reactor. With this design scheme, the TCHP system is expected to operate as an effective and stable high-temperature heat supplier for industrial process heat applications.

5. Conclusion

In this paper, a high-temperature tri-phase thermochemical heat pump is proposed to overcome the intrinsic performance constraints of conventional two-phase systems. The key parameters influencing the temperature lift, energy efficiency, and exergy efficiency of the tri-phase system are investigated on the basis of a detailed thermodynamic analysis of its multi-phase operating principles. The main conclusions are summarized as follows:

(1) The cycle boundary, i.e., the terminal sorbent state at the end of charging, is identified as the primary factor governing the performance of the tri-phase system. When the charging process is terminated at anhydrous $CaCl_2$, the energy efficiency is enhanced by up to 19.5%, and the exergy efficiency is increased by up to 34.2% compared with a conventional two-phase cycle. Under this condition, the heat released per unit mass of salt is increased by a factor of 2.6, indicating a substantial improvement in thermochemical energy density. By contrast, the most favorable temperature-lift behavior is obtained when the terminal state is $CaCl_2 \cdot H_2O$, under which a temperature lift of up to 60 °C can be achieved under the specified conditions.

(2) The evolution of the sorbent state is effectively regulated by the charging temperature, while the condensation temperature is identified as a key parameter for optimizing system performance. As the charging temperature is increased, the reaction pathway is driven toward deeper dehydration states, thereby improving the energy and exergy efficiencies of the tri-phase cycle. At the same time, an appropriate choice of condensation temperature allows the system to operate with relatively high performance while alleviating the demand on the external heat source, further decreasing the overlap of temperature range in the charging and discharging process.

(3) The further increase of discharge temperature is determined by the evaporation temperature, which directly influences through its control of the discharging pressure. As the evaporation temperature is raised, not only is the output temperature lift of the system further extended, but the exergy of heat release is also increased by 22.0%, at the expense of only a limited decrease of 1.52% in the total released heat. This behavior reflects a favorable trade-off in which a small reduction in heat quantity is exchanged for a substantial improvement in heat grade.

(4) A microencapsulation scheme for the reactive salt is considered vital for the practical development of the tri-phase system, as it guarantees the stability of the system cycle. By confining the salt solution and crystalline phases within selectively permeable microcapsules, stable, repeatable tri-phase operation is ensured, thereby enabling the proposed tri-phase concept to be realized as a technically viable engineering system.

Overall, the tri-phase thermochemical heat pump represents a promising scheme for industrial high-temperature, large-temperature-lift heat supply. To further advance its development, dedicated system prototyping and experimental testing are still required to verify its practical engineering value, which constitutes an important direction for future work.

Acknowledgements

The authors would like to thank the support of the National Natural Science Foundation of China (No. 52206033) and Beijing Natural Science Foundation (No.3232039).

References

[1] H. M. Wikoff, D. Garfield, S. Hwang, M. M. Ribo, M. Ruth, and S. B. Reese, "Benchmarking thermal energy storage cost for industrial process heat," *Applied Energy,* vol. 402, p. 126873, 2025/12/15/ 2025, doi: https://doi.org/10.1016/j.apenergy.2025.126873.

[2] H. Jouhara, A. Żabnieńska-Góra, B. Delpech, V. Olabi, T. El Samad, and A. Sayma, "High-temperature heat pumps: Fundamentals, modelling approaches and applications," *Energy,* vol. 303, p. 131882, 2024/09/15/ 2024, doi: https://doi.org/10.1016/j.energy.2024.131882.

[3] X. Ma *et al.*, "Application of absorption heat transformer to recover waste heat from a synthetic rubber plant," *Applied Thermal Engineering,* vol. 23, no. 7, pp. 797-806, 2003/05/01/ 2003, doi: https://doi.org/10.1016/S1359-4311(03)00011-5.

[4] K. Abrahamsson, A. Gidner, and Å. Jernqvist, "Design and experimental performance evaluation of an absorption heat transformer with self-circulation," *Heat Recovery Systems and CHP,* vol. 15, no. 3, pp. 257-272, 1995/04/01/ 1995, doi: https://doi.org/10.1016/0890-4332(95)90010-1.

[5] I. N. Balderas-Sánchez, W. Rivera, and J. C. Jiménez-García, "Thermodynamic analysis of a novel absorption heat transformer," *Applied Thermal Engineering,* vol. 162, p. 114268, 2019/11/05/ 2019, doi: https://doi.org/10.1016/j.applthermaleng.2019.114268.

[6] Z. Ma, H. Bao, and A. P. Roskilly, "Performance analysis of ultralow grade waste heat upgrade using absorption heat transformer," *Applied Thermal Engineering,* vol. 101, pp. 350-361, 2016/05/25/ 2016, doi: https://doi.org/10.1016/j.applthermaleng.2016.02.002.

[7] J. Ji and M. Ishida, "Behavior of a two-stage absorption heat transformer combining latent and sensible heat exchange modes," *Applied Energy,* vol. 62, no. 4, pp. 267-281, 1999/04/01/ 1999, doi: https://doi.org/10.1016/S0306-2619(99)00012-4.

[8] N. Giannetti, N. Inoue, S. Yamaguchi, and K. Saito, *Multistage Type-II Absorption Heat Pump For Steam Generation Up To 180°C*. 2018.

[9] F. Ziegler, "State of the art in sorption heat pumping and cooling technologies," *International Journal of Refrigeration,* vol. 25, no. 4, pp. 450-459, 2002/06/01/ 2002, doi: https://doi.org/10.1016/S0140-7007(01)00036-6.

[10] J. Feng, J. Gao, B. Hu, R. Wang, and Z. Xu, "A mass-coupled hybrid absorption-compression heat pump with output temperature of 200 °C," *Energy,* vol. 312, p. 133608, 2024/12/15/ 2024, doi: https://doi.org/10.1016/j.energy.2024.133608.

[11] J. T. Gao, Z. Y. Xu, and R. Z. Wang, "Enlarged temperature lift of hybrid compression-absorption heat transformer via deep thermal coupling," *Energy Conversion and Management,* vol. 234, p. 113954, 2021/04/15/ 2021, doi: https://doi.org/10.1016/j.enconman.2021.113954.

[12] Q. Ji, Y. Yin, G. Huang, D. Zhao, and B. Cao, "An advanced cascade method for optimal industrial heating performance in hybrid heat pump," *Energy Conversion and Management,* vol. 303, p. 118187, 2024/03/01/ 2024, doi: https://doi.org/10.1016/j.enconman.2024.118187.

[13] X. Hu, S. Zhang, Z. Peng, S. Tang, and N. Liu, "Dynamic Modeling and Operation Characteristics Analysis of LiBr Absorption Heat Pump," *E3S Web of Conferences,* vol. 257, p. 01022, 01/01 2021, doi: 10.1051/e3sconf/202125701022.

[14] S. Salehi, M. Yari, S. M. S. Mahmoudi, and L. G. Farshi, "Investigation of crystallization risk in different types of absorption LiBr/H2O heat transformers," *Thermal Science and Engineering Progress,* vol. 10, pp. 48-58, 2019/05/01/ 2019, doi: https://doi.org/10.1016/j.tsep.2019.01.013.

[15] B. Michel and M. Clausse, "Design of thermochemical heat transformer for waste heat recovery: Methodology for reactive pairs screening and dynamic aspect consideration," *Energy,* vol. 211, p. 118042, 2020/11/15/ 2020, doi: https://doi.org/10.1016/j.energy.2020.118042.

[16] Y. B. Fan, L. Jiang, X. J. Zhang, X. G. Xu, and A. Frazzica, "Heat pump assisted open three-phase sorption thermal battery for efficient heat storage," *Energy Conversion and Management,* vol. 277, p. 116630, 2023/02/01/ 2023, doi: https://doi.org/10.1016/j.enconman.2022.116630.

[17] N. Yu, R. Z. Wang, Z. S. Lu, L. W. Wang, and T. F. Ishugah, "Evaluation of a three-phase sorption cycle for thermal energy storage," *Energy,* vol. 67, pp. 468-478, 2014/04/01/ 2014, doi: https://doi.org/10.1016/j.energy.2013.12.044.

[18] K. E. N'Tsoukpoe, N. Le Pierrès, and L. Luo, "Numerical dynamic simulation and analysis of a lithium bromide/water long-term solar heat storage system," *Energy,* vol. 37, no. 1, pp. 346-358, 2012/01/01/ 2012, doi: https://doi.org/10.1016/j.energy.2011.11.020.

[19] L. Wang, X. Liu, Z. Yang, and K. R. Gluesenkamp, "Experimental study on a novel three-phase absorption thermal battery with high energy density applied to buildings," *Energy,* vol. 208, p. 118311, 2020/10/01/ 2020, doi: https://doi.org/10.1016/j.energy.2020.118311.

[20] J. You, J. Gao, R. Wang, and Z. Xu, "High-density and anti-clogging three-phase absorption heat storage with crystallization management," *Applied Energy,* vol. 376, p. 124240, 2024/12/15/ 2024, doi: https://doi.org/10.1016/j.apenergy.2024.124240.

[21] R. Chen, D. Lu, T. Shen, and M. Gong, "A new dynamic control strategy for a solar-driven absorption thermal energy storage system: Modeling and performance evaluation," *Applied Thermal Engineering,* vol. 260, p. 124983, 2025/02/01/ 2025, doi: https://doi.org/10.1016/j.applthermaleng.2024.124983.

[22] M. Molenda, M. Bouché, M. Linder, M. Blug, J. Busse, and A. Wörner, "Thermochemical Energy Storage for Low Temperature Applications: Materials and First Studies in a Gas-Solid Reactor," 2012.

[23] Z. Liu, D. Lu, T. Shen, R. Cheng, R. Chen, and M. Gong, "Improving heat supply of ammonia-water absorption heat transformer by enlarging heat source utilization temperature span," *Energy,* vol. 280, p. 128219, 2023/10/01/ 2023, doi: https://doi.org/10.1016/j.energy.2023.128219.